ELSEVIER

PII: S0032-3861(97)00329-7

Polymer Vol. 39 No. 3, pp. 659–667, 1998

0032-3861/97/$17.00+0.00

Small angle X-ray scattering analysis of crazing in rubber toughened polymers: Influence of particle deformation

Chaobin He[a], Athene M. Donald[a,*], Michael F. Butler[a] and Olivier Diat[b]
[a]*Polymers and Colloids Group, Cavendish Laboratory, University of Cambridge, Cambridge CB3 0HE, UK*
[b]*ESRF, BP 220, F-38043 Grenoble, France*
(Received 6 November 1996; revised 13 February 1997)

Recently, methods have been developed to characterise the relative amounts of crazing and non-crazing processes which occur in rubber toughened glassy polymers, using the invariant obtained from small angle X-ray scattering (SAXS) analysis. In this approach, however, the influence of the deformation of the rubber particles has previously been ignored. In this paper we explore how deformation of a three layer core–shell rubber particle affects such analysis. It is shown that, for a submicron rubber particle system, the form factor makes a significant contribution to the SAXS pattern, and the intensity of this scattering increases as the concentration of rubber particles increases. The details of such form factor scattering are frequently inaccessible, as the scattering occurs at very low angles. However, various extrapolated forms for this low q scattering have previously been assumed in order to calculate the amount of crazing by suitable subtraction of it from the experimental data to yield the appropriate invariant. Since the form factor may change during deformation, as the particles change shape and internal debonding or cavitation may occur, subtracting the scattering from the undeformed form factor may or may not be an adequate approximation. This paper tests the validity of the approximation. It is shown that, for our particular system, the length scale of the internal morphology of the rubber particles is comparatively large compared with the size of the crazes, and the effect of the particle deformation is indeed fairly minor. However, it is clear that with other systems, a changing form factor may overlap significantly with the peak due to crazing. This effect will then become significant and must be taken into account. © 1997 Elsevier Science Ltd.

(Keywords: small angle X-ray scattering; invariant; form factor)

INTRODUCTION

Small angle X-ray scattering (SAXS) is potentially useful for the study of deformation microstructure; not only does this method have none of the disadvantages of transmission electron microscopy (e.g. the use of ultra-thin samples), but the use of high intensity synchrotron radiation allows the possibility of an in-situ deformation study. A new method of SAXS analysis[1,2] allows a more complete separation of crazing and non-crazing processes than earlier methods, so that quantification of the contribution from crazing and non-crazing to the total deformation can be made. This quantitative analysis of SAXS is based on the evaluation of the scattering invariant using a two phase model for the craze, where the polymer fibrils and the voids between the fibrils are the first and second phases, respectively[3].

The application of the SAXS invariant to crazing analysis has been investigated by Paredes and Fischer[4], and later by Brown and Kramer[5]. If the crazes are the only scattering centres in a polymer system, the SAXS pattern will resemble a cross, as shown in *Figure 1*. If the tensile axis is vertical then the equatorial scattering will correspond to the scattering from the craze fibrils, and its intensity can be quantitatively related to the concentration of crazes, while the meridional scattering represents the scattering from craze–bulk interfaces. Unlike the equatorial scattering, the meridional scattering cannot be quantitatively related to the extent of crazing and was termed 'anomalous scattering'. In theory, to perform invariant analysis for crazes, integration of the scattered intensity over the whole q range and at all angles should be carried out. However, since the scattering from craze fibrils only appears on the equator due to their geometry, it is sufficient to carry out the integration only along the equator. This avoids the complication of dealing with the anomalous scattering on the meridian, which cannot be quantitatively related to the amount of crazing.

However, in a rubber toughened system there may be processes other than crazing contributing to the SAXS pattern, such as cavitation of rubber particles, and even the undeformed rubber particles themselves will contribute to the overall scattering. In previous studies of crazing based on invariant analysis, the scattering of the undeformed sample has been subtracted from that of the deformed one. This is an oversimplification, since the deformation of the rubber particles has been shown also to lead to changes in the SAXS pattern[6]. The shape of the scattering pattern becomes elliptical, being elongated on the equator and compressed on the meridian. More importantly, the deformation of the core–shell particles (which we have previously shown to be inhomogeneous) also leads to a significant change in the distribution of the scattering intensity along the meridian and equator[6]. The question of how the form factor scattering changes within the region (shown by the box in *Figure 1*) for which the integration of intensity is carried out, and whether it has a significant effect on the invariant analysis is therefore important. There has

* To whom correspondence should be addressed

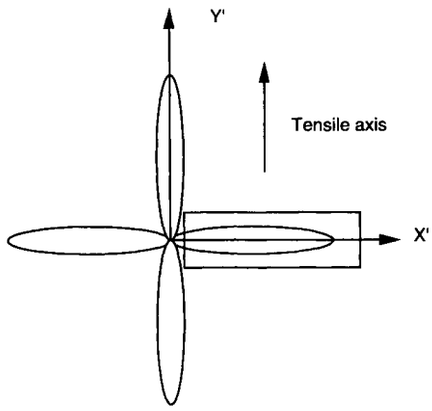

Figure 1 Schematic representation of the small angle X-ray scattering from crazes. With the tensile axis vertical, the scattering from craze fibrils is concentrated on the equator

been no previous systematic study of the influence of deformation of rubber particles on the invariant analysis. The only previous attempt to account for changes in the low q scattering upon deformation[2], *assumed* an extrapolated form, supposing that the particular particles used (different from the ones used in this paper) had voided and hence that their scattering could be described by fitting to Porod's law for a single void size. This paper will address the question of the validity of using undeformed scattering data from the rubber particles to analyse scattering for the deformed system, using simulation and experimental data, with the aim of setting up a framework for further data analysis.

EXPERIMENTAL

Model rubber toughened PMMA samples were supplied by ICI plc with five different concentrations of rubber particles ranging from 10 to 50 wt%. The rubber particles had a three layer structure: a PMMA core of 80–85 nm radius, a rubber middle layer of 40–50 nm thickness and a thin outer PMMA layer (required to ensure good adhesion between particle and PMMA matrix). The toughening particles were prepared by sequential emulsion polymerisation, and the rubber layers comprised a copolymer of *n*-butylacrylate and styrene. The ratio of *n*-butylacrylate to styrene was 4:1 by weight. In this instance crosslinking was achieved within the rubber layers by use of allylmethacrylate at a level of 5% by weight of the total rubber layer mass. SAXS methods were used to study the deformation of the polymers using the high brilliance beamline (ID2-BL4) at the synchrotron radiation source at the European Synchrotron Radiation Facility (ESRF), Grenoble (France). The sample preparation and the experimental set up have been described in the previous report[6]. Polymer samples were stretched using a Miniature Materials Tester ('Minimat' from Rheometrics Limited) with a fixed extension rate of 0.5 mm min^{-1} at room temperature. The tensile curve and X-ray scattering data were recorded simultaneously. The sample to detector distance was 10 m and the 2-D detector covered a q ($q = 2\pi/d$) range from 0.005 to 0.05 $Å^{-1}$. Data were collected during 6-s time frames and each sample had 30–50 frames of data.

SCATTERING FROM AN ORIENTED ELLIPSE

In order to understand the possible contribution of different processes to the total scattering, the scattering from different types of deformation of the rubber particle have been calculated. These allowed us to compare the SAXS from a deformed core–shell particle with that from an undeformed one.

SAXS from deformed particles (ellipses) has been extensively studied by several authors[7–12], who were mainly concerned with the overall scattering from an assembly of randomly oriented ellipses. The results have been presented as a one-dimensional scattering profile, i.e. the relation between the scattered intensity (I) and the scattering angle (q). However, since the use of invariant analysis for crazes should be confined to the equator (within the box in *Figure 1*), only the portion of the form factor within this specific region in a 2-D scattering pattern is of interest. Furthermore, in this situation the ellipses are not randomly oriented but aligned. Thus, a 2-D scattering pattern for a deformed particle (ellipse) should first be calculated, and then the relevant contribution to the scattering intensity on the equator be evaluated. A 2-D X-ray scattering pattern for an ellipse can be calculated from the Fourier transform of the electron density of the ellipse (shown in Appendix A). The result is as follows:

$$F(\xi,\eta) = \frac{\sqrt{2\pi}k\rho a^{3/2}\Gamma(1)}{[\xi^2+(k\eta)^2]^{3/4}} J_{3/2}\left[a\sqrt{\xi^2+(k\eta)^2}\right] \quad (1)$$

$$I(\xi,\eta) = F(\xi,\eta)F^*(\xi,\eta) = |F(\xi,\eta)|^2 \quad (2)$$

(the terms are defined in Appendix A)

Equation (2) represents the scattering intensity from an elliptically deformed particle with a density of ρ in vacuo. The geometries represented by the variables in equation (1) are shown in *Figures 2 and 3*.

$J_{3/2}$ is a 3/2 order of Bessel function, k is the eccentricity (ratio of long to short axis of the ellipse) and a is the length of the short axis. Assuming that the particle volume remains

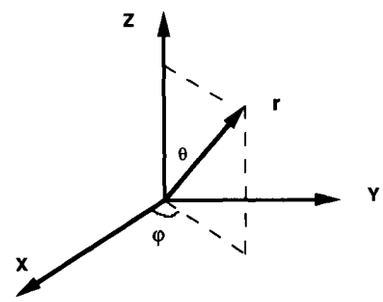

Figure 2 Schematic representation of the set of coordinates used in real space

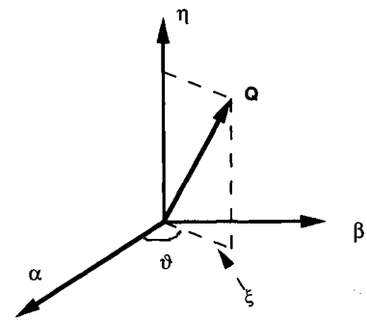

Figure 3 Schematic representation of the set of coordinates used in Q space

constant during deformation, then:

$$\frac{4}{3}\pi abc = \frac{4}{3}\pi R^3$$

where a, b, and c are the axes of the ellipse, and R is the radius of the undeformed particle. For uniaxial extension, $a = b$, $c = ka$, and $a = R(1/k)^{1/3}$.

Because only a very low q region is of interest in these experiments, the position in q space (ξ,η) can be used to represent the real space position in detector (x', y') as shown in *Figure 1*.

For a deformed core–shell particle in a polymer matrix, the densities of the PMMA core and the rubber shell are different. The extent of deformation may also differ for the two components[6]. The X-ray scattering from this body can be calculated by simply adding and subtracting the scattering from the different scattering regions (rubber particle and core particle). In the system studied here, the core–shell rubber particles consist of a three layer structure, a PMMA core, a rubber middle layer and an outer PMMA shell. Since the outer PMMA shell is identical to the polymer matrix, the density differences which give rise to the small angle scattering are between the PMMA core and the rubber layer, and the rubber layer and PMMA matrix. This can be modelled as shown in *Figure 4*.

In this figure ρ_1 is the density of the polymer matrix; ρ_2 is the rubber density and Ω_2 is the volume of the rubber as if there were no PMMA core; ρ_3 and Ω_3 are the density and volume of the PMMA core. The outer PMMA layer is indistinguishable from the PMMA matrix and causes no scattering. The Fourier transform for such a core–shell particle in a polymer matrix is therefore:

$$F(\xi,\eta) = \int_0^\infty \rho(\underline{r}) e^{i\underline{r}\underline{q}} \mathrm{d}\underline{r} \tag{3}$$

hence according to Ref. [6]

$$F(\xi,\eta) = (\rho_2 - \rho_3)\left(\int_0^{\Omega 2} e^{i\underline{r}\underline{q}}\mathrm{d}\underline{r} - \int_0^{\Omega 3} e^{i\underline{r}\underline{q}}\mathrm{d}\underline{r}\right) \tag{4}$$

$$F(\xi,\eta) = \frac{(\rho_2-\rho_3)\sqrt{2\pi}\Gamma(1)}{[\xi^2+(k\eta)^2]^{3/4}}\left(k_2 a_2 J_{3/2}\left[a_2\sqrt{\xi^2+(k_2\eta)^2}\right] - k_3 a_3 J_{3/2}\left[a_3\sqrt{\xi^2+(k_3\eta)^2}\right]\right) \tag{5}$$

where k_2 and k_3 are the eccentricities for Ω_2 and Ω_3, respectively and a_2 and a_3 are the lengths of the short axes for Ω_2 and Ω_3, respectively.

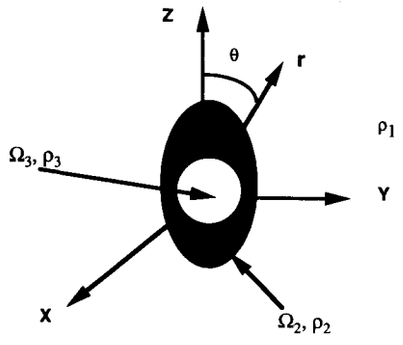

Figure 4 Schematic representation of a deformed core–shell particle in a polymer matrix

RESULTS AND DISCUSSION

Calculation of the relative invariant

The total scattered intensity arising from the craze fibrils (i.e. that contained within the rectangular box in *Figure 1*) is evaluated in two steps. First, for each value of x', integration along the y' axis was carried out. Typically there were about 30 to 40 pixels in the y' direction and therefore this integration has the effect of slit smearing, although the synchrotron itself is point collimated. In the second stage of the analysis the slit-smeared data are integrated along x' (x' is the scattering angle ($= 4\pi\sin\Theta/\lambda$)).

The method for analysing quantitatively the total craze volume is based on the theory[3] that for smeared intensity data $I_c(x')$, the integral

$$\mathrm{INV_c} = \int_0^\infty I_c(x')x'\mathrm{d}x' \tag{6}$$

is a constant (or invariant) for a two phase model with only two types of scatterers. It is independent of the geometry of these scatterers and only depends on the total volume of scattering centres. This idea has been utilised in the context of crazing[4,5] and it has been suggested that by evaluating the invariant, the concentration of crazes can be found.

Experimentally, the results are recorded as 2-D SAXS data. The calculation of the invariant is then performed by integrating the intensity within the equatorial rectangular area. The area for these experimental conditions is defined as $0.005\ (X_{\min}) < x' < 0.05\ (X_{\max})\ \text{Å}^{-1}$ and $-0.004\ (\text{Å}^{-1}) < y' < 0.004\ (\text{Å}^{-1})$. The integral then becomes:

$$\mathrm{INV_c} = 2\int_{X_{\min}}^{X_{\max}}\left[\int_0^{0.004} I_c(x',y')\mathrm{d}y'\right]x'\mathrm{d}x' + \mathrm{INV_{tail}}$$

$$\mathrm{INV_c} = 2\int_{X_{\min}}^{X_{\max}} I_c(x')x'\mathrm{d}x' + \mathrm{INV_{tail}} \tag{7}$$

where $\mathrm{INV_{tail}}$ represents the tail of the scattering at high q. It is worth noting that in theory the calculation of the invariant should be carried out by integrating in a q range (x' range here) from 0 to infinity. However, the very low q region and the very high q region are experimentally inaccessible. The method described here is equivalent to that used by Bubeck *et al.*[1].

For the higher angle scattering, Porod analysis can be used to calculate the contribution to the integral ($\mathrm{INV_{tail}}$) and has been fully discussed previously[1,3–5]. In our study, we used the final 50 data points to calculate the Porod constant K, using a plot of Iq^3 *versus* q. (It should be noted that although the source itself is not slit smeared, the analysis of the high q data has been integrated along the y axis over about 40 pixels, as described earlier for the lower q data. This form of Porod's law—correct for slit smeared data—is therefore the correct one.) The contribution of the high angle region ($X_{\max} < q < \infty$) to the invariant is:

$$\mathrm{INV_{tail}} = \frac{2\pi K}{X_{\max}}$$

Since the craze scattering has a maximum at a comparatively high angle ($\sim 0.03\ \text{Å}^{-1}$), the ultra low angle scattering will not have a significant effect on the invariant analysis and can therefore be ignored.

Influence of deformation of rubber particles

It has been shown[6] that in a rubber toughened polymer matrix, the experimentally obtained equatorial scattering,

$I_t(x',y')$, not only consists of scattering from the crazes, $I_c(x',y')$, but also of scattering from the rubber particles themselves, $I_f(x',y')$. Supposing that the scattering from core–shell rubber particles is independent of the scattering from crazes, then we have:

$$I_c(x',y') = I_t(x',y') - I_f(x',y') \tag{8}$$

$$\mathrm{INV_c} = 2\int_{X_{min}}^{X_{max}}\left[\int_0^{0.004} I_c(x',y')\mathrm{d}y'\right]x'\mathrm{d}x'$$

$$= 2\int_{X_{min}}^{X_{max}}\left[\int_0^{0.004} I_t(x',y')\mathrm{d}y'\right]x'\mathrm{d}x' \tag{9}$$

$$- 2\int_{X_{min}}^{X_{max}}\left[\int_0^{0.004} I_f(x',y')\mathrm{d}y'\right]x'\mathrm{d}x'$$

The subtraction of the contribution of the form factor from the experimental data is, however, complicated by the fact that the rubber particles also deform to some extent. The deformation of the rubber particles not only alters the shape of the SAXS pattern (from a circle to an ellipse), but also changes the intensity (shown in *Figure 5*(1)–(9), with the corresponding load–extension curve in *Figure 6*; a discussion of the variation in intensity of such patterns has been discussed previously[6]). *Figure 7* shows a one-dimensional cut through the scattering from the undeformed particle, and for comparison the simulated form factor scattering based on an individual particle of the same dimensions. This figure shows clearly that the rings do indeed arise from the form factor scattering.

Two questions arise if we are to be able to perform this subtraction: how does the form factor change as the particle deforms and is there any relation between the scattering from an undeformed particle and a deformed one?

Experimental methods alone cannot give a satisfactory answer to the above questions, since the experimental data contain contributions from all the different effects. An effective way to model this problem is via computer simulation. Since the total scattering from the craze fibrils occurs on the equator, the main concern of invariant analysis is the scattering in this direction. The main objective of the simulation carried out here is therefore to see how the form factor changes within the equatorial rectangular area when the rubber particles deform, so that this effect can be separated from the scattering from crazes. The scattering from a deformed core–shell particle with different degrees of deformation of the rubber layer and PMMA core can be calculated according to equations (5) and (10). Hence the contribution of the form factor to the total scattering intensity within the rectangular area can be analysed by numerical calculation. In this simulation, we only considered a single core–shell rubber particle in a polymer matrix, regardless of the particle size distribution and any interparticle interference. The deformation ratio is referred to the real rubber particle deformation, i.e. k (the ratio of the long axis to the short axis of an ellipse), but not the total extension of the sample. According to *Figure 1*, the integral of the form factor can then be calculated as:

$$2\int_{X_{min}}^{X_{max}}\left[\int_0^{0.004} I_f(x',y')\mathrm{d}y'\right]x'\mathrm{d}x' \tag{10}$$

$I_f(x',y')$ can be calculated from equation (5). *Figure 8* shows the analysis of the computer simulation results, plotted as the ratio of the integral due to the deformed particle to that of the undeformed one as a function of the deformation ratio. When keeping the core undeformed, it can be seen that the value of the integral increases with the rubber deformation. Compared with the undeformed particles, the deformed particle with $k = 1.3$ has a 20% increase in the value of the integral. If the deformation of the rubber shell is kept constant at $k = 1.4$ while changing the extent of deformation of PMMA core (bearing in mind that previous work has indicated that the core and the rubber layer do not deform homogeneously), the magnitude of the integral again increases with increasing deformation of the PMMA core, as shown in *Figure 8*. If the very low angle region is included in the simulation, for example the q range of $0.0001 < x' < 0.05$, we see a near linear relation between the extent of deformation and the ratio of the integrals, as shown in *Figure 9*. At the maximum possible deformation of the rubber particle (in our polymer system approximately $k = 1.4$ as can be seen from the SAXS in *Figure 5*) while keeping the core undeformed, the integral increases by only 7%. If the rubber layer is kept at the same extension ($k = 1.4$), the integral decreases with increasing deformation of the core. It is clear from the above two sets of data that the integral increases with increasing deformation of both the core and the shell. It is also shown that the influence of deformation of particles on the value of the integral depends on the angular region studied.

The results for the simulation can now be compared with the experimental result. Turning to the sequence of scattering patterns in *Figure 5*, we can see how the ellipticity gradually increases until fracture (marked by the point on the corresponding load–extension curve in *Figure 6*). *Figure 10* shows how the ratio of the integral of the deformed sample to that of the undeformed one changes during deformation. It first decreases and then increases steadily as the maximum extension is reached, and decreases slightly after fracture. The initial decrease of the integral may arise from interparticle interferences which are not taken into account in the simulation.

In general, the rubber layer is easily deformed while the PMMA core normally remains undeformed[13] and the experimental data should be therefore compared with simulation results for a particle with an undeformed core. The correlation between the value of the integral and the extent of particle deformation obtained experimentally agrees fairly well with the computer simulation prediction for a non-crazing polymer matrix, for which the integral was calculated in the region of $0.005 < x' < 0.05$ ($\mathrm{Å}^{-1}$).

The ratio of the integral for the deformed particle to the undeformed one is slightly higher in the computer simulations compared with the experimental results. This may be due to the simplifications inherent in the simulation, which only considers a single particle regardless of the particle size distribution and interparticle interference. Thus, we see that for a deformation of the rubber particles corresponding to $k = 1.3$, the simulation predicts an increase in the value of the integral of 20%, while the experimental data for a matrix with 50 wt% rubber particle show a 12% increase. This suggests that the majority of the contribution to the changing integral does come from a non-crazing response. This is to be expected as such a high concentration of rubber particles will tend not to promote crazing but alternative deformation mechanisms. This point will be further addressed in a subsequent paper.

Influence of crazes and cavities

However, the crucial question is whether we can accurately assess via the invariant analysis what the contribution from crazing is, by appropriate subtraction of the form factor. To this end we examine the behaviour of a matrix containing 20 wt% of particles (2-D SAXS pattern shown in *Figure 11* with the corresponding load–extension curve in *Figure 12*), since this system will be expected to show significant amounts of crazing. The calculated ratio of the integral for the deformed sample to the undeformed one is shown in *Figure 13*. Compared with the matrix containing 50 wt% of rubber particles, the particles are more resistant to deformation, as can be seen from the fact that rings arising from the form factor in *Figure 11* remain close to circular (see also the discussion in Ref. [6]). As the deformation of the particle proceeded, the value of the integral increased gradually, and finally as the polymer matrix began to yield (shown by the load–extension curve), there was a significant increase. The final value was nearly 10 times the initial value. Moreover, the intensity of the scattering after this yield point was so intense that the detector was saturated, and reliable data could not be collected thereafter. This 10-fold increase cannot be explained by the deformation of the rubber particles alone, since we have shown that it only contributed about 15–20% increase of the integral for $k = 1.3$. There are two other factors which could contribute to the increase of the integral: voiding (cavitation) and crazing.

It is worth noting that at the late stage of deformation, voiding (cavitation or debonding) occurred which had a profound effect on the scattering intensity distribution along the equator and meridian[6]. We have tried to use the numerical calculation to investigate this effect on the integral, but the convergence of the integral was too slow. Fortunately, the experimental data assisted our analysis. In a matrix with 50 wt% concentration of rubber particles, significant voiding within the particles occurred at the late stage of deformation, as shown by the detailed form of the low q (form factor) scattering. This result has been confirmed by computer simulation[6]. However, this voiding

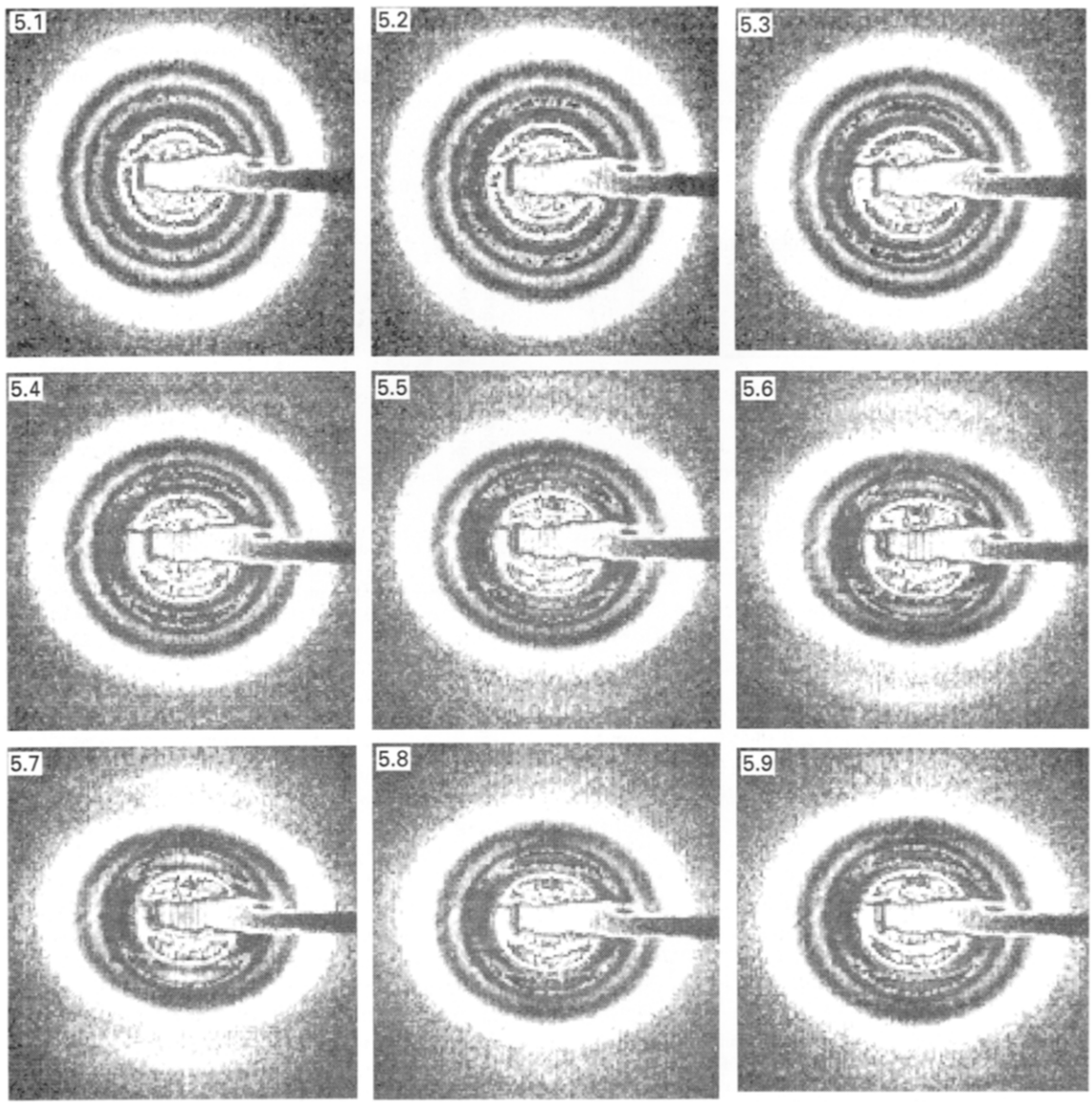

Figure 5 2-D SAXS patterns of a rubber toughened PMMA (50 wt% of rubber particles) sample strained to different degrees. Conditions used are a strain rate of 0.5 mm min^{-1} at room temperature and extensions of: (1) 0 mm; (2) 0.33 mm; (3) 0.67 mm; (4) 1.0 mm; (5) 1.33 mm; (6) 1.67 mm; (7) 1.8 mm; (8) 2.0 mm; (9) 2.07 mm, respectively. q_x and q_y range from -0.2 to $+0.2$ $Å^{-1}$

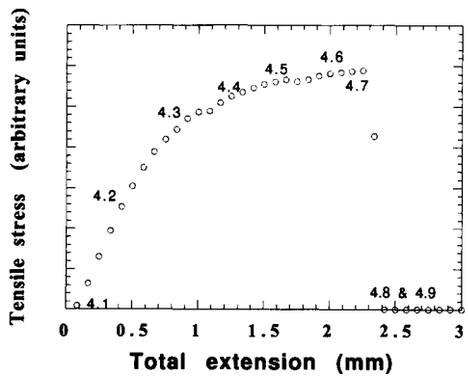

Figure 6 Load extension curve for the deformed polymer matrix with 50 wt% core–shell rubber particles shown in *Figure 5*. Due to the shape of the samples used, it is difficult to obtain an absolute value for the tensile stress, and the *y* axis is therefore in arbitrary units

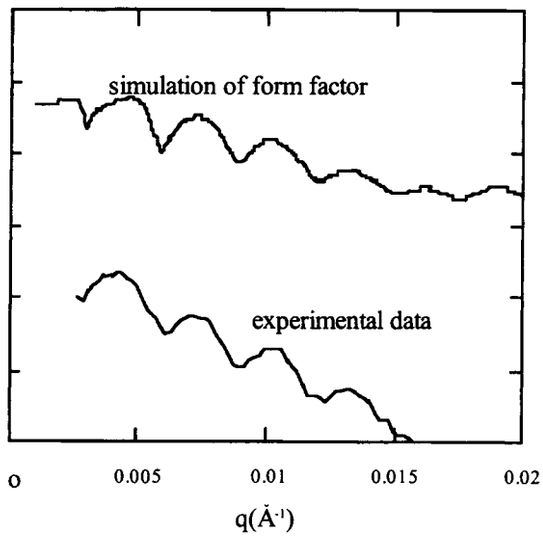

Figure 7 One-dimensional cut through the scattering pattern of an undeformed particle, compared with the simulated scattering due to the particle form factor for a particle of the same dimensions as those experimentally used. The vertical displacement between the two curves is arbitrary

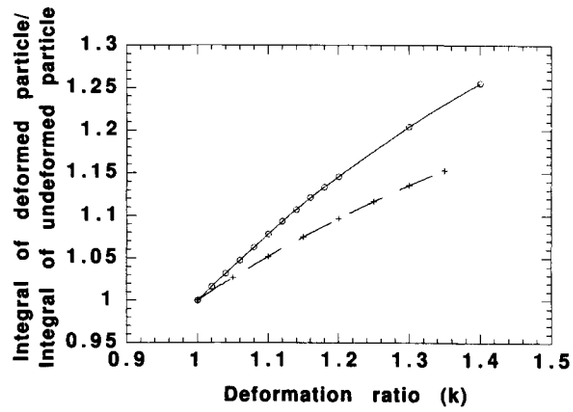

Figure 8 Computer simulation results on the influence of particle deformation on the invariant analysis for the region of $0.005 < q < 0.2$. The rubber particle consists of three layers (PMMA core–rubber layer–PMMA outer layer). Only one particle in a PMMA matrix is studied. o, The rubber layer deforms while the PMMA core remains unchanged; +, deformation of the rubber layer is kept at 40% while the core PMMA deforms

does not contribute significantly to the integral, as can be deduced from *Figure 10*. Hence, it can be concluded that voiding does not significantly affect the magnitude of the integral in our system (its intensity must be less in a system with a lower concentration of particles which could potentially void), and cannot be the reason for the 10-fold increase in the integral seen in *Figure 13*. Thus we deduce that the large increase in the integral must be attributed to the appearance of crazes in the polymer samples.

The fact that the appearance of crazes increased the value of the integral by a factor of 10 while the deformation of the core–shell particles and voiding only leads to a 12% increase, indicates the dominance of the crazing contribution. This result is reassuring since it means that, for this system at least, despite the internal structure of the particles and the way their form factor changes during deformation, the contribution to the integral is completely dominated by the crazing. It is thus sufficient in general to calculate the value of INV_c by subtracting the form factor of the undeformed particle: only a small error will be introduced by so doing. However, particularly when the concentration of crazes is very low and the internal deformation of the rubber particles is high, the influence of changing particle shape on the invariant analysis may become significant, so that the calculation of the amount of crazing may not be

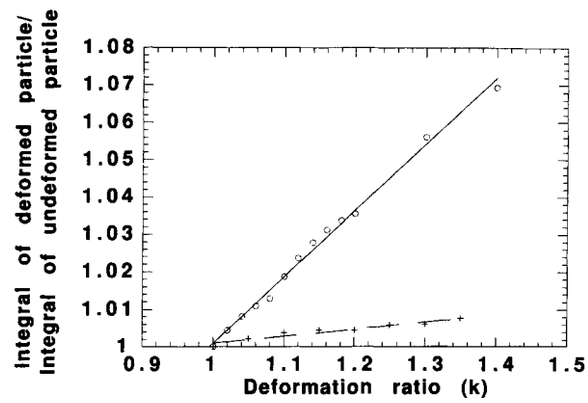

Figure 9 Computer simulation results on the influence of particle deformation on the invariant analysis for the region of $0.0001 < q < 0.2$. o, The rubber layer deforms while the PMMA core remains unchanged; +, deformation of the rubber layer is kept at 40% while the core PMMA deforms

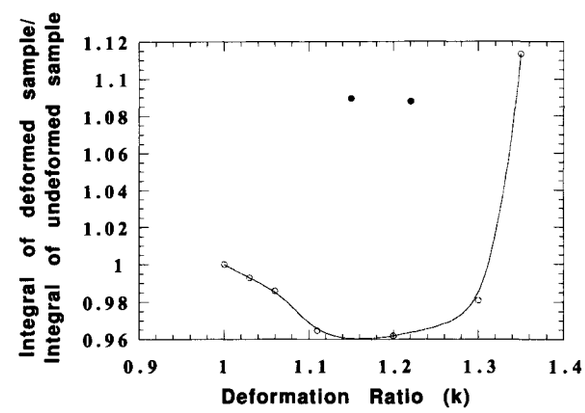

Figure 10 Experimental results on the influence of the deformation of polymer matrix with 50 wt% core–shell rubber particle on the integral according to equation (10): ○, data when the polymer matrix is under tensile strain; ●, data when the polymer matrix is broken

accurate. We estimate this will lead to a maximum deviation from the true value of 20%.

It is important to note that this calculation has been carried out for a particular system, and caution must be exercised in extending it to other systems. In the past[1,2] analysis of the contribution from crazing has been hampered by the inability to access such low scattering angle as have been possible using the ESRF. In particular, Magalhaes and Borggreve[2] had to extrapolate the low angle contribution, which was presumed to be due to internal voiding of rubber particle, before evaluating the crazing contribution. For our system we can put the invariant analysis on a sound footing, and in a subsequent paper we will use this approach explicitly to evaluate the effect of rubber particle concentration and rubber crosslinking density on the amount of crazing. However, for rubber particles with a fine-scale morphology it is possible that the form factor effect may much more directly impinge on the scattering from the crazes, rendering the approximation we have been able to make in this paper no longer valid.

CONCLUSIONS

In a rubber toughened polymer matrix (or other polymer composite systems), the scattering from the form factor of the particles must be taken into account when using the invariant analysis to calculate the craze density. The importance of the contribution of the form factor depends on the concentration of rubber particles in the polymer matrix.

The contribution of the form factor to the invariant analysis also depends on the extent of deformation since the rubber particle themselves deform; however, the change in the contribution of rubber particles to the invariant analysis upon deformation is negligible compared with crazing in our polymer system. Therefore, the data for undeformed samples can be used as an approximation of the contribution of the deformed sample to invariant analysis, as has been carried out in the past without the approximation being tested. However, if the rubber particle size or its internal morphology is smaller, the influence of the deformation of rubber particles will need to be reconsidered.

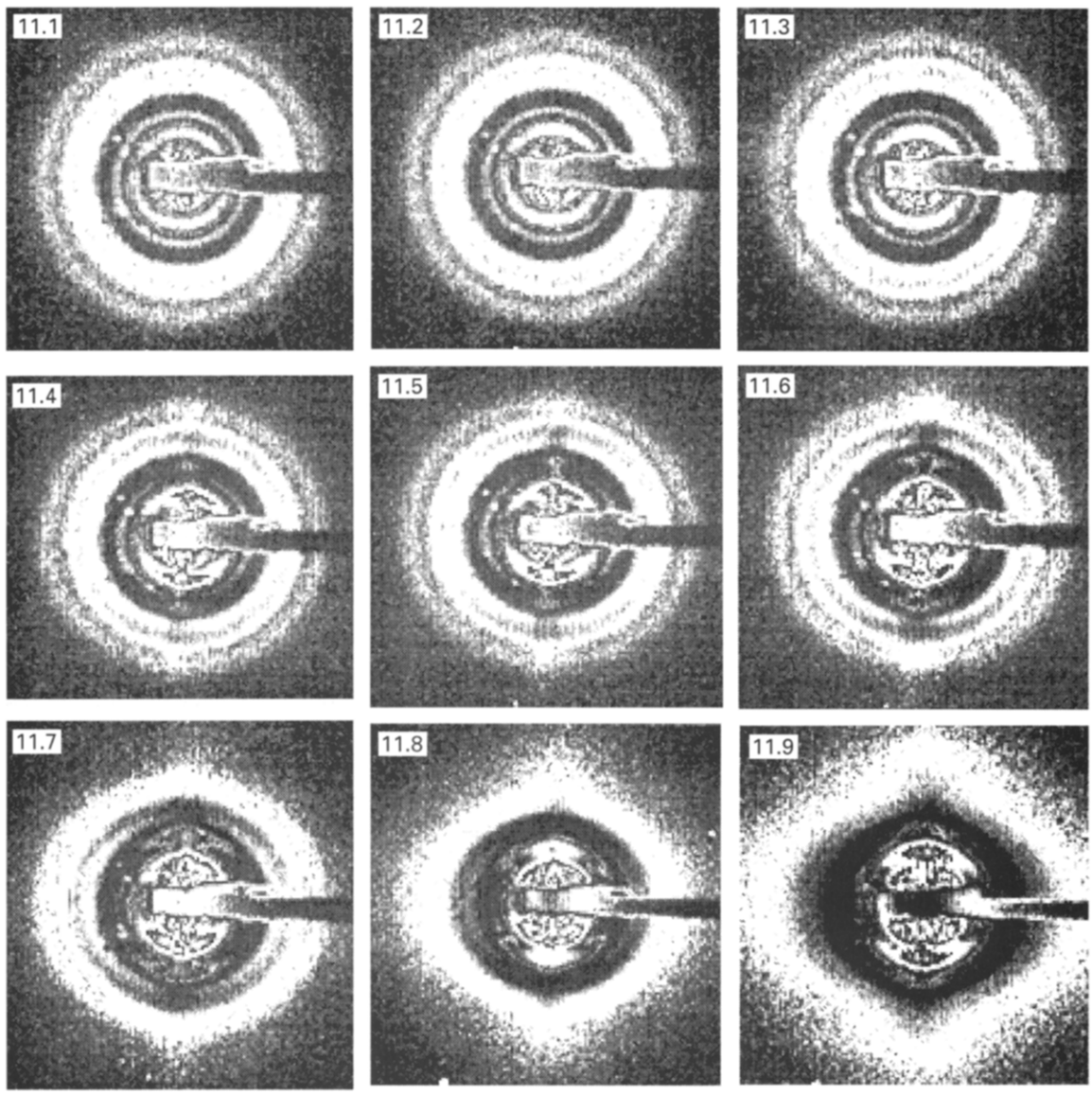

Figure 11 2-D SAXS patterns of a rubber toughened PMMA (20 wt% of rubber particles) sample strained to different degrees. Conditions used are a strain rate of 0.5 mm min^{-1} at room temperature and extensions of: (1) 0 mm; (2) 0.33 mm; (3) 0.67 mm; (4) 1.0 mm; (5) 1.07 mm; (6) 1.13 mm; (7) 1.2 mm; (8) 1.27 mm; (9) 1.33 mm

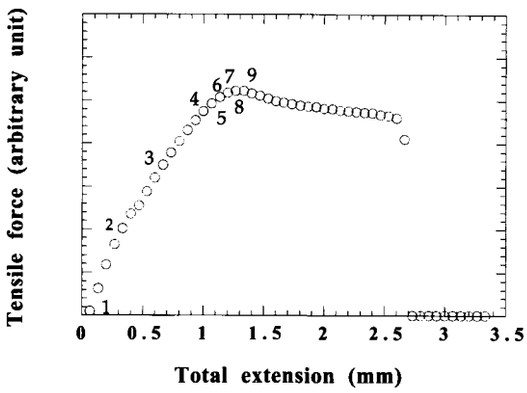

Figure 12 Load–extension curve for the deformed polymer matrix with 20 wt% core shell rubber particles shown in *Figure 10*

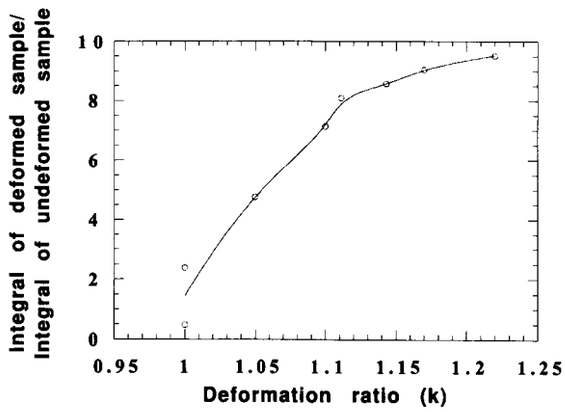

Figure 13 Experimental results on the influence of deformation of the polymer matrix with 20 wt% core–shell rubber particle on the integral according to Eq. (10)

ACKNOWLEDGEMENTS

The authors would like to thank: Dr Ian M. Fraser, ICI, for providing the polymer samples and helpful discussions, Dr Eugene Terentjev, University of Cambridge, for assistance with the mathematics, EPSRC for financial support and ESRF for providing the facilities. Tom Waigh, University of Cambridge, is thanked for helping with the experimental work at ESRF and David Johnson and Peter Bone, University of Cambridge, are thanked for helping with the production of the tensile specimens.

APPENDIX A:

For a uniaxially deformed sample, the rubber particles are stretched only in one direction. The shape of a deformed particle can be thought of as an ellipse and can be described by the volume Ω defined by:

$$x^2+y^2+\left(\frac{z}{k}\right)^2 \le a^2$$

where k is the ratio of long axis to short axis of a deformed particle (modelled as an ellipsoid, with circular cross-section) and a is the length of the short axis of the ellipse. For an undeformed particle, k is 1. *Figures 2 and 3* show the geometry of real space (the scattering body) and Q space (the scattering pattern). The relation between these two is given by the Fourier transform $F(\alpha,\beta,\eta)$:

$$F(\alpha,\beta,\eta)=\int_\Omega \rho e^{irq}\mathrm{d}\underline{r}=\int_\Omega \rho e^{i(\alpha x+\beta y+\eta z)}\mathrm{d}x\mathrm{d}y\mathrm{d}z$$

where ρ is the density of the deformed particle, which is assumed constant, and Ω defines the volume of the particle.

According to *Figure 2*, in real space, and using polar coordinates, we have:

$$x=r\sin\theta\cos\varphi\ y=r\sin\theta\sin\varphi z=r\cos\theta$$

$$F(\alpha,\beta,\eta)=k\rho\int_0^a r^2\mathrm{d}r\int_0^\pi \sin\theta\mathrm{d}\theta \times\int_0^{2\pi} e^{i[r\sin\theta(\alpha\cos\varphi+\beta\sin\varphi)+kr\eta\cos\theta]}\mathrm{d}\varphi$$

In Q space as shown in *Figure 3*, we have

$$\xi=\sqrt{\alpha^2+\beta^2}\cos\vartheta=\frac{\alpha}{\xi}\sin\vartheta=\frac{\beta}{\xi}$$

$$F(\xi,\eta,\vartheta)=k\rho\int_0^a r^2\mathrm{d}r\int_0^\pi \sin\theta e^{ikr\eta\cos\theta}\mathrm{d}\theta \times\int_0^{2\pi} e^{ir\xi\sin\theta\cos(\varphi-\vartheta)}\mathrm{d}\varphi$$

According to Ref. [14], then

$$F(\xi,\eta)=k\rho\int_0^a r^2\mathrm{d}r\int_0^\pi \sin\theta e^{ikr\eta\cos\theta}J_0(r\xi\sin\theta)\mathrm{d}\theta$$

where J_0 is the Bessel function of zero order.

We have:

$$\int_0^\pi \sin\theta\sin(kr\eta\cos\theta)J_0(r\xi\sin\theta)\mathrm{d}\theta=0$$

Then:

$$F(\xi,\eta)=k\rho\int_0^a r^2\mathrm{d}r\int_0^\pi \sin\theta\cos(kr\xi\cos\theta)J_0(r\xi\sin\theta)\mathrm{d}\theta$$

According to Ref. [15], then

$$F(\xi,\eta)=k\rho\sqrt{2\pi}\int_0^a \frac{J_{1/2}\left[r\sqrt{\xi^2+(k\eta)^2}\right]}{[\xi^2+(k\eta)^2]^{1/4}}\mathrm{d}r$$

According to Ref. [16], then

$$F(\xi,\eta)=\frac{\sqrt{2\pi}k\rho a^{3/2}\Gamma(1)}{[\xi^2+(k\eta)^2]^{3/4}}J_{3/2}\left[a\sqrt{\xi^2+(k\eta)^2}\right]$$

$J_{3/2}$ is a 3/2 order of Bessel function.

REFERENCES

1. Bubeck, R. A., Buckley, D. J., Kramer, E. J. and Brown, H. R., *Journal of Materials Science*, 1991, **26**, 6249.
2. Magalhaes, A. A. M. and Borggreve, R. J. M., *Macromolecules*, 1995, **28**, 5841.
3. Porod, G., in *Small Angle X-ray Scattering*, ed. O. Glatter and O. Kratky, Chapter 2: General Theory. Academic Press, London, 1982.
4. Paredes, E. and Fischer, E. W., *Makromolekulare Chemie*, 1979, **180**, 2707.
5. Brown, H. R. and Kramer, E. J., *Journal of Macromolecular Science—Physics*, 1981, **19B**, 487.
6. He, C., Donald, A. M., Butler, M. F. and Diat, O., *Macromolecular Symposium*, 1996, **112**, 115.
7. Guiner, A., *Annals of Physics*, 1939, **12**, 161.
8. Shull, C. and Roess, L., *Journal of Applied Physics*, 1947, **18**, 195.
9. Porod, G., *Acta Physica Austriaca*, 1948, **2**, 133.

10. Schmidt, P. W. and Hight, R. Jr., *Journal of Applied Physics*, 1959, **30**, 866.
11. Mittelbach, P. and Porod, G., *Acta Physica Austriaca*, 1962, **15**, 122.
12. Hamzeh, F. M. and Bragg, R. H., *Journal of Applied Physics*, 1974, **45**, 3189.
13. Schirrer, R., Fond, C. and Lobbrecht, A., *Journal of Materials Science*, 1996, **31**, 6409.
14. Watson, G. N., *A Treatise on the Theory of Bessel Functions*, 2nd edn. Cambridge University Press, Cambridge, 1966, 31 pp.
15. *Table of Integrals Series and Products*, ed. I. S. Gradshteyn and I. M. Kyzhik; translation by A. Jeffery. Academic Press, 1965, 743 pp.
16. *Table of Integrals Series and Products*, ed. I. S. Gradshteyn and I. M. Kyzhik; translation by A. Jeffery. Academic Press, New York, 1965, 688 pp.